APPENDIX C
CONSEQUENCE MODELING

TO THE

INDEPENDENT RISK ANALYSIS
(APPENDIX C1)

APPENDIX C

CABRILLO PORT FSRU LNG HAZARD SCENARIO CONSEQUENCE MODELING JANUARY 2006

J. Keith Clutter, Mike W. Stahl, and Charles Vergara
Analytical & Computational Energetics, Inc. (ACE)
3463 Magic Dr, Ste. 359, San Antonio, TX 78229
210.582.5860
www.aceng.net

1 INTRODUCTION

Because of the volumes being considered for transportation, storage, and processing at the proposed Cabrillo Port LNG FSRU, there is a need to evaluate the potential consequences from accidents or intentional acts. To better understand these consequences, modeling of potential LNG spills and resulting fires or explosions were analyzed. The modeling techniques employed, the assumptions made, and the results are presented below.

The theoretical physical and thermal processes involved in an LNG spill are shown in Figure 1. Figure 2 is an event tree that identifies the different potential hazards that could occur after the LNG is spilled. Following a spill, the resulting pool could either be ignited and a pool fire will result, or the pool will begin to evaporate. If the vapor cloud produced during a spill evaporates and disperses, it may encounter an ignition source and produce a fire or an explosion. Each of these events, within the context of the Cabrillo Port facility, is addressed in this document. The section numbers noted in Figure 2 show the particular section of this document that addresses that event.

Each of these processes shown in Figure 1 must be represented in the analysis, and the particular method depends in part on the modeling tool used. The choice of modeling tool depends on factors such as local conditions, environmental factors, including the presence of structures, and other site-specific items. The output from the various models is dependent on the inputs and assumptions used to represent the physical event. The underlying modeling assumptions can also affect the results. Here the modeling input parameters used are clearly defined. In each section the reader is guided to appropriate references that present the details of the methodology behind the various models used.

This document presents various consequences and hazard distances for a range of potential LNG spillages. The release scenarios considered were defined as part of a larger risk assessment conducted for the Cabrillo Port facility.

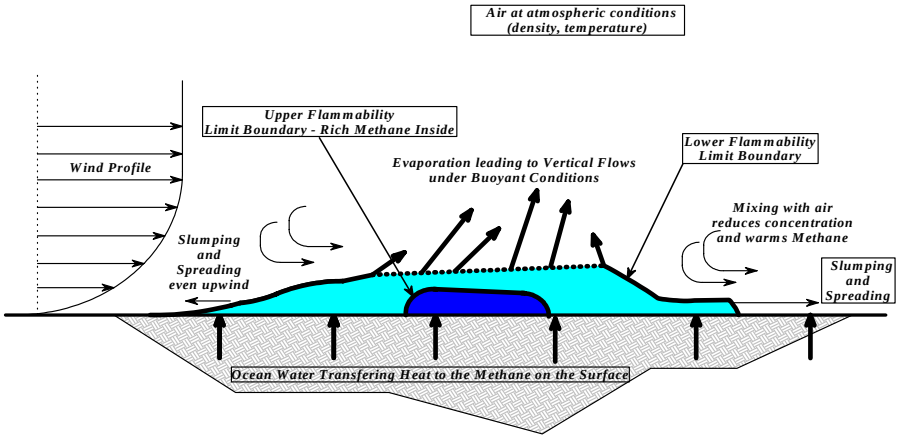

Figure 1. Notional figure showing the LNG dispersion process.

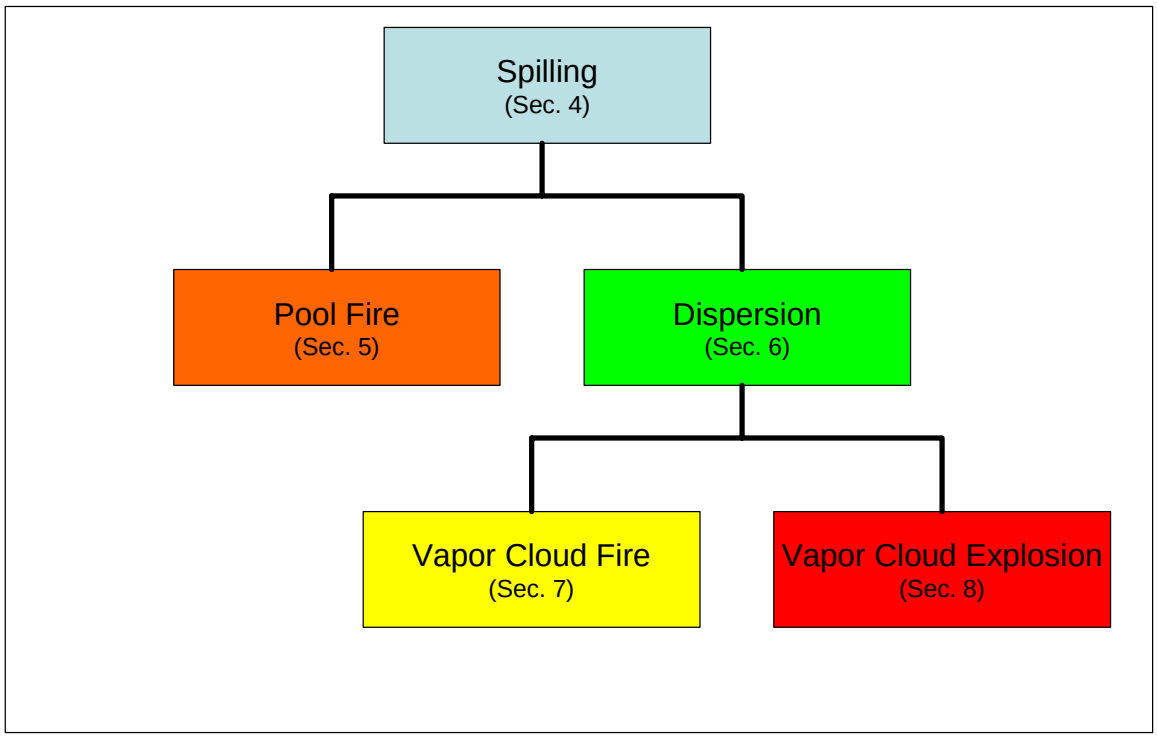

Figure 2. Event tree showing potential hazards after the spilling of LNG. Noted is the section of this document that addresses each event.

1.1 Dispersion Model Description

Of particular interest in the current study was the potential dispersion of flammable gas from the spill. This was due to the fact that the location of the proposed facility is some distance from

shore. Therefore, the potential migration of gas to the shore needed to be addressed. To date, a popular analysis method used when considering LNG is the application of the Dense Gas Dispersion Model (DEGADIS), which was developed for the U.S. Coast Guard, the Gas Research Institute, and the U.S. Environmental Protection Agency. DEGADIS is based on analytical and empirical methods and was specifically developed for heavier-than-air gases or aerosols. Natural gas, which LNG becomes after evaporation, is lighter than atmospheric air and thus does not fall within this class. For justification regarding the use of DEGADIS for LNG applications, the reader is referred to the work of Haven and Spicer [1].

Based on all the processes involved in the potential FSRU LNG spill scenarios, the decision was made to use a computational fluid dynamics (CFD) modeling tool to simulate the dispersion process. This approach is consistent with the recommendations found in guidance developed by Sandia National Laboratories [2]. The various inputs and assumptions used in the modeling are defined along with results. Below is a brief description of the tool and validation data.

The model used for liquid and gas dispersion is the Fire Dynamics Simulator (FDS) developed by the National Institute of Standards and Technology (NIST) [3]. FDS is a CFD code that solves the full set of governing equations for fluid motion. Though developed primarily for fire simulations, it has been successfully used for a broader range of fluid dynamics problems. As evident in the Burro 8 and 9 studies described in Chang [4] and Clement [5], it can predict the dispersion of liquids and gases with good accuracy. FDS was selected for use here in part because it is a publicly available code and therefore can be used by any party interested in modeling LNG spill scenarios. The reader is directed to McGrattan [3] to learn more on the details of the model's mathematical assumptions and formulation.

As with any CFD code, there are various options when using FDS. Some are related to how the various physical processes are represented. The physical inputs used for the simulations are provided in Section 3 of this report. Equally important are the numerical aspects of the model. One numerical aspect is the grid spacing; grid spacings used in the simulations are defined with the results.

A second numerical aspect is the boundary conditions as they are applied at the boundaries of the computational domain used. There are three basic options: (1) defining the variable values at the boundary, (2) defining derivative conditions at the boundary, or (3) treating the boundary as a mirror where no flux is allowed across the boundary. The mirror boundary conditions were used for the simulations presented in this document. An extensive modeling study found that the best option for use in FDS was to apply mirror boundary conditions also on the "side" and "roof" boundaries. The location of these boundaries was set such that the flow and dispersion of gas was not adversely affected.

1.2 Fluid Dynamic Processes Influencing Dispersion

When considering the dispersion of evaporated LNG, various fluid dynamic processes affect the downwind distance to which the released gas will migrate. The first is the speed of the wind, which works to convect the gas downwind at a certain rate. Also important are the buoyancy

effects that will cause the gas to migrate vertically. The final process is dissipation, which is a function of the velocity gradient and will "thin out" the gas as it moves downwind.

Wind speed plays an important role in the time history of the cloud formation and its movement downwind. Buoyancy effects play the same role but in the vertical direction. Because these are competing processes, wind speed or misrepresentation of buoyancy effects can lead to mistakes in downwind hazard distances. If the dissipation is overestimated, the downwind vapor cloud dispersion distances will be underestimated because the gas cloud will be thinned out too early.

Numerous simulations were conducted to better understand the representation and role of the various fluid dynamic processes. It was found that the dissipation, which is directly tied to the wind velocity profile, played a large role. Therefore, lower wind velocities were used during the simulations to ensure that the wind profile and dissipation process were adequately represented and that the hazard distance was not underestimated.

When using the CFD-type model, representation of the wind velocity profile throughout the computational domain is somewhat different from the traditional empirically based models such as DEGADIS. This is because in the CFD code, velocity can only be specified at a boundary. Since the governing equations are solved only at discrete points, the velocity field can change during the computational process. To determine the adequacy of the dissipation process representation in the current study, the gradient in velocity, as measured normal to the bottom of the computational domain, was analyzed for all cases. The wind velocity gradient as calculated by the code was compared to the value based on the wind velocity profile at the upstream boundary. The wind velocity profile was taken from meteorological data. If the calculated magnitude of the gradient from the code was close to or less than the analytical data, then it could be concluded that the dissipation process is adequately represented. The velocity gradient information is presented for each simulation.

2 DISPERSION BENCHMARK

Prior to simulation of the cases specific to the Cabrillo FSRU, the FDS was tested using benchmark data from the Burro 8 test executed by the U.S. Department of Energy [6]. As discussed in Havens [1], this data has been used to assess the validity of many dispersion modeling tools. Of particular interest is the prediction of the maximum distance to the lower flammability limit (LFL) as compared to that measured in the Burro 8 tests. During the Burro 8 tests, the average wind direction was approximately 10 degrees from the centerline of the sensor array. The spill for Burro 8 was 28.4 cubic meters (m^3) for 113.3 seconds. The atmospheric stability recorded during the Burro 8 test was slightly stable and the average wind speed was 1.8 meters per second (m/s) at an elevation of 10 meters (m).

During the Burro 8 test, gas concentrations were recorded at different elevations above ground surface. The probe towers are located in lines that project radially from the point of release. The sampling stations are at distances of 57, 140, 400, and 800 m from the release point. Each tower has probes at 1, 3, and 8 m above ground. The data from the Burro data series described in Koopman [6] was interrogated, and the line running from the release point along which the maximum recorded distance to LFL was used. The recordings from the different probes are

shown in Figure 3 and 4. Denoted in the plots is the concentration level corresponding to LFL. The data from the 8 m high probes are not shown since the recordings at that elevation were below LFL across the complete range of data.

Also shown for comparison are data from the Burro 9 test. The test conditions for Burro 9 were similar to those for Burro 8, except that during the Burro 9 test, the average wind direction was 7 degrees from the centerline of the sensor array and the average wind speed was 5.7 m/s at an elevation of 10 m. The spill flow rate was 24.2 m^3/s for 130.3 seconds. The atmospheric stability was similar in that it was neutral stable. The spills were similar enough that the maximum probe readings occurred on the same line of probes in both tests.

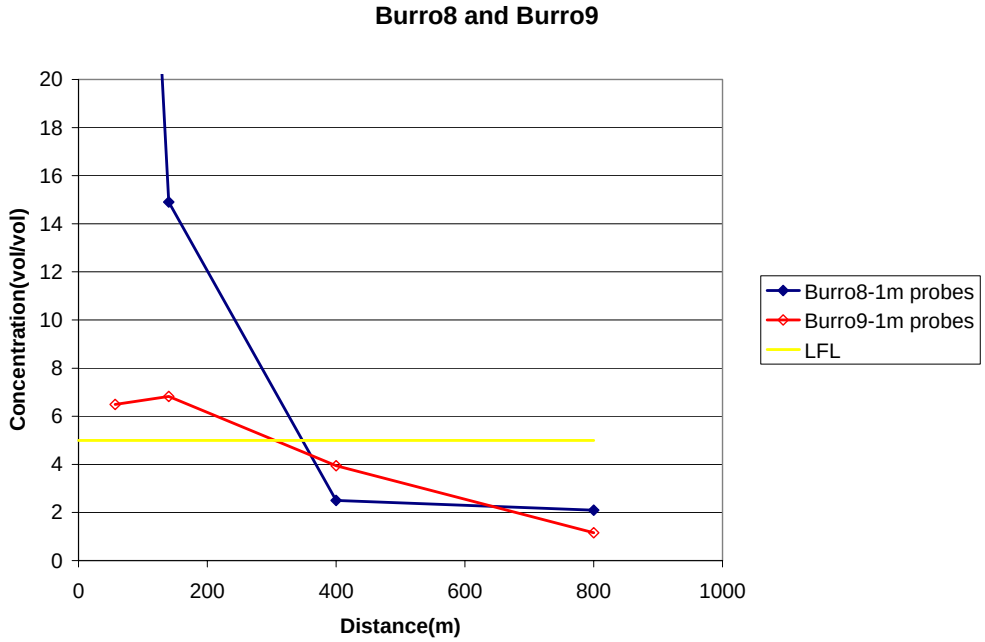

Figure 3. Gas concentration data recorded 1 m above the ground during the Burro 8 and Burro 9 tests.

The test data show that the wind speed affects the maximum distance to LFL. However, it is not solely the magnitude of the wind speed, but the change (or gradient) in velocity moving vertically, normal to the ground. This will affect dissipation and is discussed later. The probes stationed 3 m above the ground (Figure 4) recorded the maximum distances to LFL in both cases. The exact location for the maximum LFL distance falls between the locations of actual measurements, but can be estimated to be between 250 m and 500 m. Accounting for the orientation of the array of probes relative to the wind direction and using the original test data to interpolate, the maximum distance to LFL for the Burro 8 case has been estimated by Sandia National Laboratories to be approximately 420 m. [7].

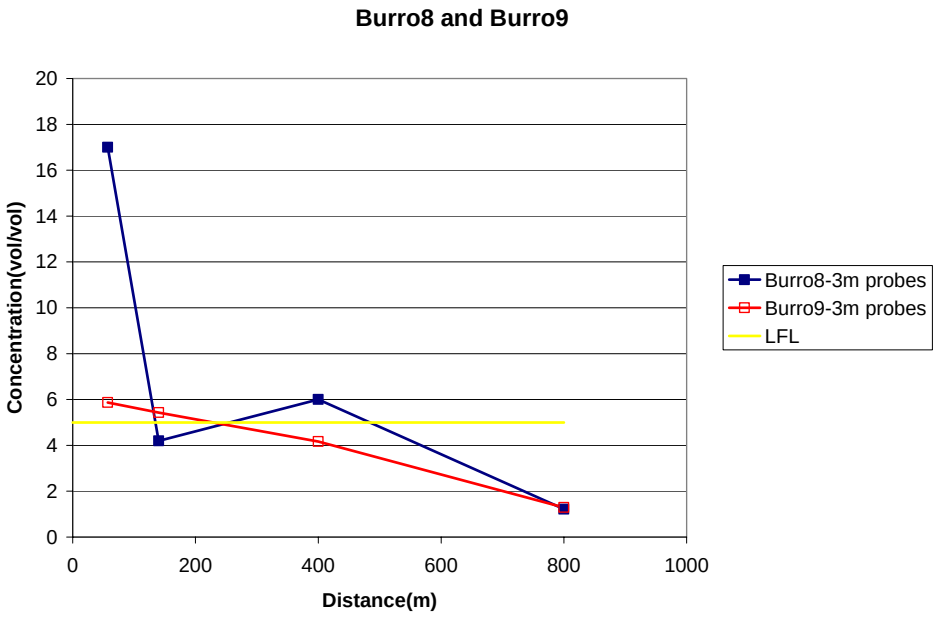

Figure 4. Gas concentration data recorded 3m above the ground during the Burro 8 and Burro 9 tests.

To simulate the Burro 8 scenario, the grid spacing used was (dx, dy, dz) = (5 m, 5 m, 1 m) over a domain covering a footprint of 1,200 m by 500 m. In the Burro 8 test, LNG was spilled on a pool of water causing it to cover the complete surface of the pool. The concentration of natural gas was measured at several stations downwind of the pool, and the data show that the largest distance at which the gas maintained a concentration at or greater than the LFL was approximately 420 m. Natural gas is approximately 95 percent methane. Therefore, the values for flammability limits associated with methane in air were used. For methane in air, the LFL is 0.0276 on a mass fraction basis or 0.05 on a volume fraction basis.

This release was simulated in FDS by specifying a pool size equal to that in the tests. Natural gas was released off the pool area at a rate equal to the evaporation rate of the LNG recorded in the tests. For the simulation, the average wind profile as measured in the test was imposed at the upwind boundary of the domain. The wind profiles measured in the tests and used in the simulation are shown in Figure 5. Also shown are the corresponding velocity gradients normal to the ground plane. During the simulation, the distance to where gas concentration maintained a level at least as high as the LFL was recorded. The simulation results showed the maximum downwind distance to LFL to be approximately 490 m. This is within 14 percent of the test measurements, which is well within the spread of the test data recorded in the dispersion tests described by Koopman [6]. Figure 5 shows a plan view snapshot of the gas as it reached the final downwind distance.

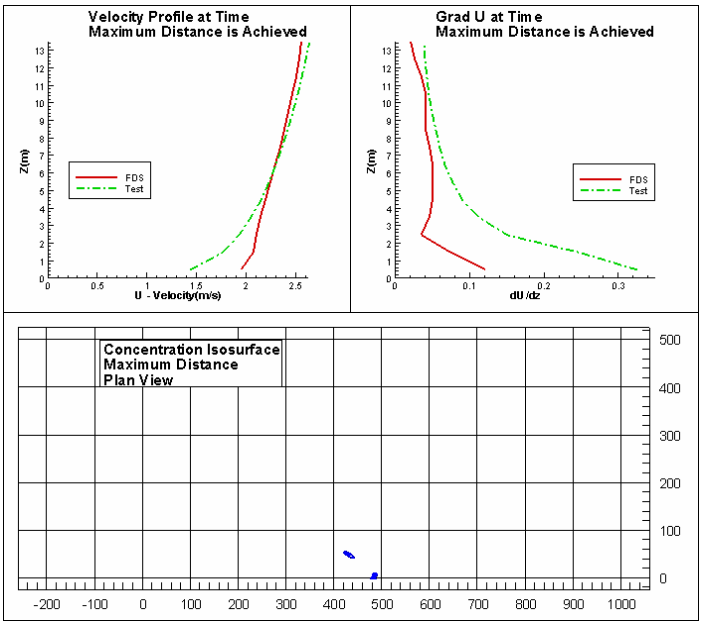

Figure 5. Prediction for the Burro 8 test case in which LNG was spilled on a pool of water and the resulting dispersed vapor cloud was recorded.

3 PHYSICAL INPUT PARAMETERS

To represent the various processes involved in the potential LNG events, several physical input parameters need to be set. These include environmental factors such as wind, atmospheric, and ocean conditions, as well as parameters affecting the spilling of the LNG, such as pool size, in setting hazard distances. This section is a summary and explanation of how various parameters were selected and represented in the current simulations.

3.1 Winds and Profiles

The wind speeds used in the Cabrillo specific simulations were selected based on information provided from buoys near the planned FSRU location. To model wind speed in the simulation a velocity was imposed at the upwind edge of the computational domain. This was accomplished by using the *vent* option in FDS at the boundary with the speed and direction of the wind specified.

Along with the wind's speed and direction, a velocity profile was specified to describe the offshore conditions. During the risk assessment, it was found that the wind profile over the open water abided by a power law profile with an exponential of 0.15. The FDS inputs at the upwind boundary were set to reproduce this profile as close as possible.

3.2 Ambient Temperatures

To model the LNG spills and dispersions, the ambient air temperature and surface temperature of the water were defined within the model. These temperatures were obtained from meteorological

information for the area in which the FSRU is to be positioned. The ambient air temperature was set to 21°C while the surface temperature was set to 10°C.

When using the CFD-type model for the simulation, the ambient air temperature can change locally based on its interaction with other material in the domain. For example, the cold natural gas vapor will affect the local air temperature. Likewise, the warmer air will affect the released vapor. This is important since the warming of the natural gas will affect its buoyancy characteristics.

The ambient surface temperature was set to represent the ocean temperature. Because the ocean body is so large, there is no appreciable heating of the majority of the water mass. This is represented within the simulation by not allowing the surface temperature to change.

3.3 Hole sizes

For the various threat scenarios considered, two primary hole sizes were introduced in the storage tanks. The first, a hole with an area of 7 square meters (m^2), was used for the intentional scenario. For the marine collision scenario, the hole was much larger and specified to be approximately one-eighth of the tank's surface area, which is approximately 1300 m^2. This was defined by analysis documented in Appendix D of the Cabrillo Port Independent Risk Assessment.

3.4 Tank Releases and Spills

A variety of release scenarios were considered and several references are made to the time delay between the opening of the holes introduced in the tanks. The following discusses how these were represented within the model.

Instantaneous: An instantaneous release is a spill that originates from one or more tanks before any other significant dispersion or fire processes occur. Tanks that dump their contents instantaneously are modeled in the CFD program with a hole already built into the tank. The simulation originates with the LNG spilling from holes in the tanks. The maximum diameter of the pool formed by an LNG spill is determined by the mass balance of material lost from the pool with the mass added to the pool from the tank spill. The loss of mass from the pool can be due to either fire or evaporation. For cases such as this one, analytical methods can be used with confidence because there are no timing or flow interaction issues of importance. The pool formations predicted by the CFD models compare well to predictions from the analytical methods.

Simultaneous: Simultaneous releases are modeled by allowing more than one tank to dump its contents at the same time. The interaction between the two flows can be somewhat complicated and will affect the pool formation. This is not easily handled with analytical techniques, but it can be represented with a CFD code. The additional flow from the second tank increases the maximum pool diameter because a mass balance is not achieved until a larger pool is formed.

Escalation: A scenario is considered to be one of escalation if the contents of additional tanks are released at some time after an initial tank release has started. This type of scenario was a primary driver for using CFD to model the release of material from the tanks. The added dynamics of multiple streams interacting and the growth and retraction of the pool is not easily represented with the analytical models.

To represent the material release in an escalation situation, the appropriate tanks were modeled and filled with material. The first tank had a hole in the tank of the desired size while the additional tanks were constructed with wall sections that would be removed during the simulation at a specified time. This can be modeled using FDS. The delay time was determined based on a mass balance of the material release from the first tank and the pool size. The time at which a maximum size was achieved also was determined. Using this information, a second simulation was conducted, and the second and/or third tanks were set to release their contents at the specified delay time. Mass balance was then used to determine the maximum pool diameter. A summary of all release scenarios considered is provided in Table 1.

Table 1. Summary of release scenarios considered.

Case	Number of Tanks	Time Delay After Tank 1 Release (sec)	Hole Size in Tank (m^2)			Percent of Tank Inventory Spilled		
			1	2	3	1	2	3
Collision	1	-	1,300	-	-	50	-	-
Intentional	2	0	7	7	-	100	100	-
Escalation	2	25	7	1,300	-	100	50	-
Escalation	3	25	7	1,300	1,300	100	50	50

4 SPILLING

Based on the range of scenarios considered and to represent all the aspects of the releases as mentioned earlier, FDS was selected because it has been proven useful for such scenarios, as described in Clement [5]. The release simulations tracked the size of the pool as it formed. Using an evaporation rate of 0.135 kilograms per square meter per second ($kg/m^2/s$), the point when the growth of the pool would end due to mass balance was calculated.

To verify that the calculations were reasonable, comparisons of FDS results for non-escalation events were made with several analytical methods such as that based on the work of Raj [8]. The FDS calculations were consistent with the predictions from the analytical methods. The spill calculations had good agreement with results generated by Sandia National Laboratories [2].

Using the CFD model to calculate the pool formation allowed the same modeling approach to be used for all release scenarios, including the escalation cases. These cases will potentially occur when the pool formed from the spill of one tank catches fire and structurally weakens a second and possibly a third tank. This would result in the release of additional material and would produce a larger pool, thereby increasing the hazard.

In an escalation scenario where more than one tank is releasing its contents sequentially, the pool size and duration will depend on when the subsequent tanks release their inventory. To maintain a pool size equal to or larger than that formed by the spilling from the first tank, the follow-on

spills must occur before the diameter of the initial pool begins to shrink due to mass balance. After performing several simulations, it was determined that at approximately 25 seconds after the release from the first tank, the diameter of the initial pool began to reduce. Therefore this was the delay time selected when considering subsequent releases in an escalation scenario.

To cover the range of intentional events and marine collision possibilities, four release cases were considered. The maximum pool diameters were determined for each based on the defined hole sizes. Table 2 provides a summary of pool sizes and the key parameters of hole size and mass loss rate.

Table 2. Summary of pool sizes from the various releases.

Threat	Hole Size	Mass Balance Type	Mass Loss Flux ($kg/m^2/s$)	Maximum Pool Diameter (m)
Marine collision	Half of one side	Evaporation	0.135	730
2 tank intentional	7 m^2 holes in each tank	Evaporation	0.135	650
2 tank escalation	7 m^2 hole in 1st tank, 1,300 m^2 in 2nd tank	Pool fire	0.282	610
3 tank escalation	7 m^2 hole in 1st tank, 1,300 m^2 in 2nd and 3rd tanks	Pool fire	0.282	800

5 POOL FIRE

One potential occurrence after the spill of LNG is a pool fire. The thermal radiation resulting from pools formed by the marine collision and intentional event scenarios were considered. The pool fires were modeled using the Right Circular Cylinder Method described in the SFPE Handbook of Fire Protection Engineering [9]. Although CFD type models have proven useful and accurate in pool fire analysis, as presented in McGrattan [3], they have not been fully benchmarked against pool sizes on the order of those considered here. Therefore, a different analytical type of model was selected based on Sandia National Laboratories guidance [2].

The analytical models require the definition of various physical parameters. To determine the hazard distance for the current study, an average emissive power of 220 kilowatts per square meter (kW/m^2) and an atmospheric transmissivity of 0.8 were used based on Sandia National Laboratoreis guidance [2]. The flame height was found using the Moorhouse correlation allowing for the calculation of radiative flux to locations of interest. It should be noted that equation for the Moorhouse correlation as presented in the SFPE Handbook of Fire Protection Engineering [9] contains a misprint—the leading factor should be 6.2 instead of 62. For the release scenarios considered, the distances to radiative flux values of interest are provide in Table 3.

For this study, the radiative fluxes of interest are 37.5 kW/m^2, 12.5 kW/m^2, and 5 kW/m^2. These were used because they represent radiative flux at which equipment damage and personal injury can occur. The 37.5 kW/m^2 contour represents damage to process equipment including steel tanks and chemical process equipment, as well as immediate death for unprotected exposure. The 12.5 kW/m^2 contour represents the minimum energy to ignite wood with flame, melt plastic

tubing, and cause serious injury after 30 seconds. The 5 kW/m^2 contour is the level for emergency operations lasting several minutes with appropriate clothing.

The pool fires resulting from three potential escalation cases were considered. Each was initiated with a 7 m^2 hole present in one of the LNG storage tanks. The spill from this tank was formed and ignited. In the first case, it was assumed that a 7 m^2 hole formed in a second tank approximately 25 seconds after ignition. This time delay was selected based on the pool formation criteria discussed earlier. The second escalation case assumed that approximately one-eighth (1,300 m^2) of the wall surface of the second tank failed and resulted in additional spilling. The final escalation case assumed that after the 25 second delay two additional tanks failed with one-eighth of their wall surfaces opening. A summary of distances to the critical values of heat flux for these cases is given in Table 3. Of the scenarios considered, the largest hazard was produced by the three-tank escalation case and had a pool fire distance of 3,230 m.

Table 3. Distances to radiative flux levels of interest for various release scenarios.

			Distance to Specified Flux Level (m)		
Case	**Vol. (m^3)**	**Pool Dia. (m)**	**37.5 kW/m^2**	**12.5 kW/m^2**	**5 kW/m^2**
Marine collision	50,000	730	910	1,830	2,970
2 tank intentional	200,000	650	810	1,620	2,640
Escalation 2 tanks (7 m^2 + 1,300 m^2)	150,000	610	770	1,540	2,510
Escalation 3 tanks (7 m^2 + 2 x 1,300 m^2)	200,000	800	1,000	1,990	3,230

6 DISPERSION

In addition to potential pool fires, additional hazards could occur if spilled LNG were to evaporate and disperse downwind. This scenario could result in a large vapor cloud fire or explosion. FDS was selected to simulate the dispersion based on reasons such as those presented in the Sandia guidance document [2]. Processes such as buoyancy are included in CFD-based models. This is important for lighter than air gases such as natural gas.

Vapor clouds formed from the spills resulting from the intentional event and the marine collision scenarios were considered. The escalation cases were not included since all terminated in pool fires. For all the vapor cloud cases, the LNG evaporation rate was set to be 0.135 kg/m^2/s with the temperature of the natural gas vapor being -162°C at the pool surface. The vapor cloud was tracked as it developed with time, allowing for the determination of the maximum distance downwind at which a flammable gas concentration was recorded. This location was based on interrogating the simulation results to determine those points where the mass fraction of natural gas was at least 0.0276, the LFL for a natural gas and air mixture.

For the intentional event scenario, the LNG pool had a diameter of approximately 650 m. Within the FDS model, an equivalent area was defined and the evaporation of the LNG was represented using the appropriate material flux rates. Simulations were performed for different wind velocity fields. In each the velocity magnitude at 10 m elevation was specified. The velocity was assumed to vary according to a power law of 0.15. For the case of U = 6 m/s, a grid with spacing (dx, dy,

dz) = (25 m, 25 m, 5 m) produced a maximum distance to LFL of approximately 8,280 m. A plan view of the cloud when this distance is reached can be seen in Figure 6. The importance of the velocity profile and resulting gradient field were discussed earlier. Information regarding these aspects of the simulation is also shown in Figure 6. The velocity profiles downwind of the release are affected by the release as would be expected. The curve labeled "Test Data" is the ideal profile as defined by the assumed wind speed and power law shape.

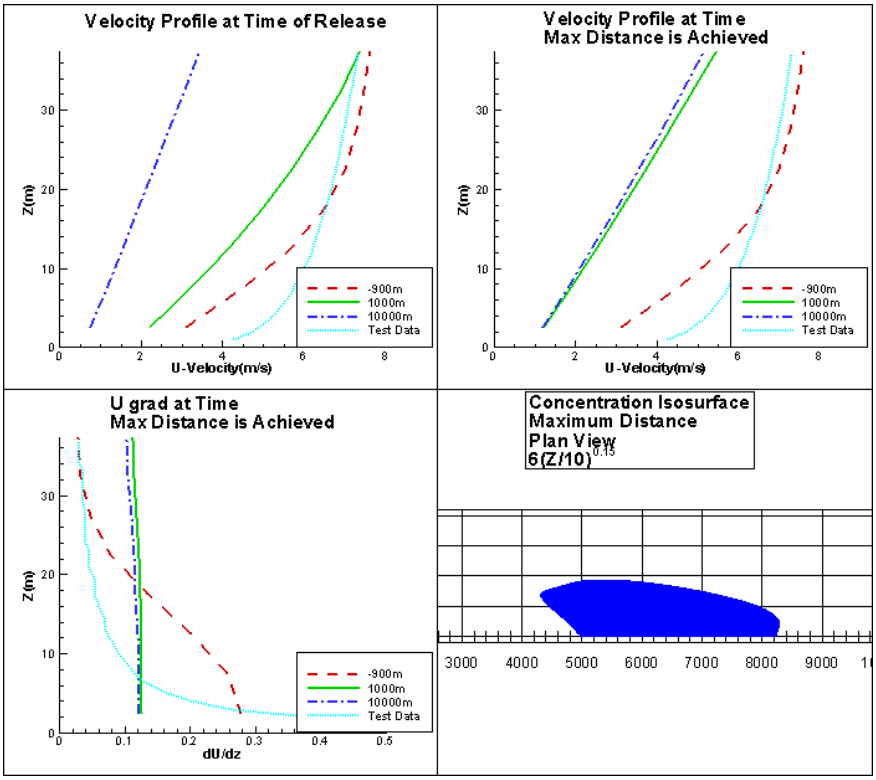

Figure 6. Predicted release out of two tanks, each with holes, into a 6 m/s wind field.

Figure 7 shows when a release from the same 650 m diameter pool is simulated to occur into a wind field where the velocity at the 10 m elevation point is 4 m/s. Using grid spacing of (dx, dy, dz) = (25 m, 25 m, 5 m), the maximum distance to LFL is approximately 9,420 m. And if the wind speed at the 10 m mark is adjusted down to 2 m/s, the maximum distance to LFL is found to reach approximately 11,175 m. These results were generated using grid spacing (dx, dy, dz) = (20 m, 20 m, 20 m) and are shown in Figure 8.

Also considered was the dispersion from the marine collision scenario. For this case, it was assumed that only half the inventory in a single tank spilled. Using a wind speed of 2 m/s, a maximum downwind distance to LFL of approximately 5,300 m was predicted. The shorter distances as opposed to the intentional event scenario cases are due to the lower inventory. All results are summarized in Table 4.

To model the dispersion process with FDS, the various parameters reviewed in Section 3 have to be established. As an example, Table 5 provides the input data required to run FDS for the

release scenario involving two tanks, each with a 7 m^2 hole present. The line numbers have been added and are not part of the file. Table 6 provides a line-by-line description of the various parameters.

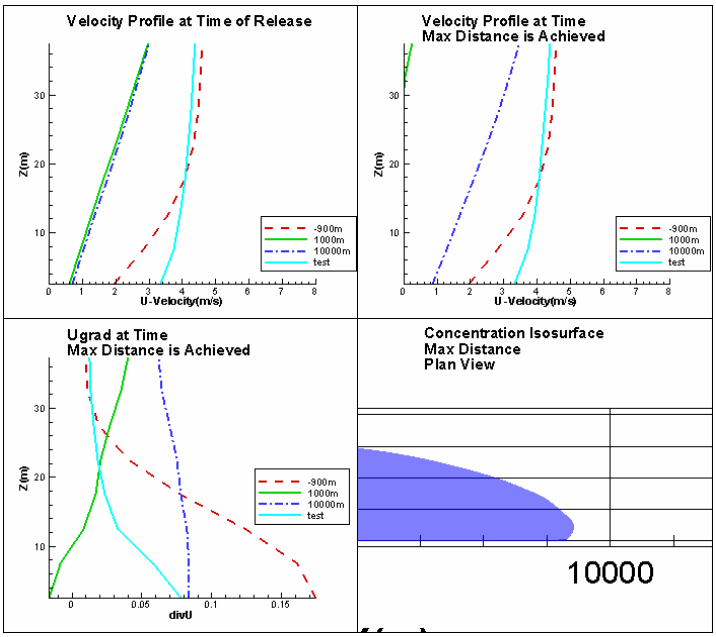

Figure 7. Release predictions for the 4 m/s wind condition.

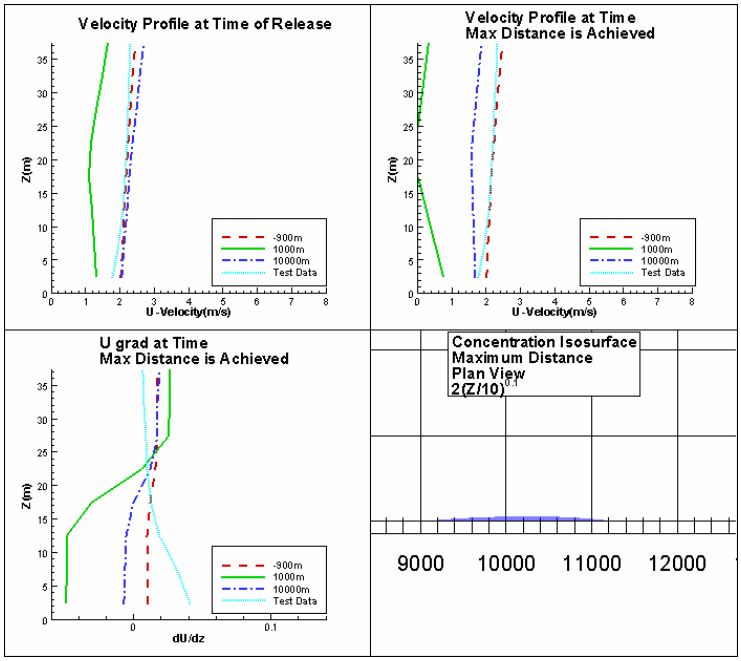

Figure 8. Predicted release into the 2 m/s wind condition.

Table 4. Summary of dispersion cases considered.

Case	Number of Tanks	Volume (m^3)	Pool Diameter (m)	Hole Size in Tank		Wind Speed (m/s)	Max. Distance to LFL (m)
				1	2		
Marine collision	1 tank	50,000	730	1,300 m^2	-	2	5,290
Intentional	2 tanks	200,000	650	7 m^2	7 m^2	2	11,175
Intentional	2 tanks	200,000	650	7 m^2	7 m^2	4	9,420
Intentional	2 tanks	200,000	650	7 m^2	7 m^2	6	8,280

Table 5. Example of FDS input file.

```
1   &HEAD CHID='fds', TITLE='cabrillo 2t 2-7m^2 holes' /

2   &GRID IBAR=710, JBAR=125,KBAR=20 /
3   &PDIM XBAR0=-1000,XBAR=14000,YBAR=3000,ZBAR0=0,ZBAR=400 /

4   &TRNY CC=1800.0,PC=1500.0 /

5   &TIME TWFIN=200000 /

6   &SPEC ID='CH4',MW=16,DENSITY=1.72 /

7   &MISC LES=.TRUE.,BACKGROUND_SPECIES='AIR' TMPA=21 U0=2  /

8   &SURF ID='Wind', VEL=-2,PROFILE='ATMOSPHERIC',Z0=10,PLE=0.15 /
9   &SURF ID='WATER',TMPWAL=10 /
10  &SURF ID='LID',TMPWAL=21, VBC=1 /
11  &SURF ID='CH4' MASS_FLUX(1)=0.135 TMPWAL=-161 /

12  &VENT CB='XBAR0',SURF_ID='Wind'/
13  &VENT CB='XBAR',SURF_ID='OPEN'/
14  &VENT CB='YBAR0',SURF_ID='MIRROR'/
15  &VENT CB='YBAR',SURF_ID='MIRROR'/
16  &VENT CB='ZBAR0',SURF_ID='WATER'/
17  &VENT CB='ZBAR',SURF_ID='LID'/

18  &VENT XB=-60,610,0,70,0,0,SURF_ID='CH4',T_OPEN=2000,T_CLOSE=4039/
19  &VENT XB=-50,590,70,120,0,0,SURF_ID='CH4',T_OPEN=2000,T_CLOSE=4039/
20  &VENT XB=-30,570,120,150,0,0,SURF_ID='CH4',T_OPEN=2000,T_CLOSE=4039/
21  &VENT XB=-10,540,150,195,0,0,SURF_ID='CH4',T_OPEN=2000,T_CLOSE=4039/
22  &VENT XB=14,500,195,230,0,0,SURF_ID='CH4',T_OPEN=2000,T_CLOSE=4039/
23  &VENT XB=40,455,230,260,0,0,SURF_ID='CH4',T_OPEN=2000,T_CLOSE=4039/
24  &VENT XB=66,400,260,280,0,0,SURF_ID='CH4',T_OPEN=2000,T_CLOSE=4039/
25  &VENT XB=110,340,280,295,0,0,SURF_ID='CH4',T_OPEN=2000,T_CLOSE=4039/
26  &VENT XB=150,300,295,310,0,0,SURF_ID='CH4',T_OPEN=2000,T_CLOSE=4039/

27  &PL3D DTSAM=20,WRITE_XYZ=.TRUE.,QUANTITIES='TEMPERATURE','U-VELOCITY','V-
    VELOCITY','W-VELOCITY','CH4'/

28  &ISOF QUANTITY='CH4',VALUE(1)=0.0276 /
```

Table 6. Definition of the various parameters in the example FDS file.

1	Heading Definition (**&HEAD**) **CHID**: name of the simulation (arbitrary) **TITLE**: name of the scenario (arbitrary)
2	Grid Definition (**&GRID**) **IBAR**: defines how may grid cells are in the X-Direction **JBAR**: defines how may grid cells are in the Y-Direction **KBAR**: defines how may grid cells are in the Z-Direction
3	Domain Definition (**&PDIM**) **XBAR0**: lower dimension of the domain in the X-Direction [m] **XBAR**: upper dimension of the domain in the X-Direction [m] **YBAR0**: lower dimension of the domain in the Y-Direction [m] **YBAR**: upper dimension of the domain in the Y-Direction [m] **ZBAR0**: lower dimension of the domain in the Z-Direction [m] **ZBAR**: upper dimension of the domain in the Z-Direction [m]
4	Grid Stretching in the Y-Direction (**&TRNY**) **CC**: computational coordinate where stretching begins **PC**: physical coordinate where stretching begins
5	Time **(&TIME**) **TWFIN**: computational time that the simulation will run [s]
6	Species Definition **(&SPEC**) **ID**: unique identifier for the species **MW**: molecular weight of the species [g/mol] **DENSITY**: density of the species [kg/m^3]
7	Miscellaneous Model Parameters (**&MISC**) **LES**: large eddy simulation **BACKGROUND_SPECIES**: material that is already in the computational domain **TMPA**: temperature of background species [C] **U0**: initial velocity in the X-Direction of every cell [m/s]
8 to 11	Surface Definition (**&SURF**) **ID**: unique identifier for the surface **VEL**: velocity of material entering the domain, negative means entering [m/s] **PROFILE**: wind profile type **Z0**: wind velocity reference height [m] **PLE**: atmospheric profile coefficient **TMPWAL**: surface temperature [C] **VBC**: surface boundary slip condition **MASS_FLUX(n)**: mass flow rate per unit area entering through a surface [kg/m^2/s]
12 to 17	Boundary Vent Definition **(&VENT**) **CD**: boundary being defined **SURF_ID**: defines which &SURF ID's properties are applied to the boundary vent
18 to 26	Vent Definition **(&VENT**) **XB**: defines the vent footprint's dimensions [m] **SURF_ID**: defines which &SURF ID's properties are applied to the vent **T_OPEN**: the computational time that the vent starts releasing material [s] **T_CLOSE**: the computational time that the vent stops releasing material [s]

27	Plot3D Output File Definition (**&PL3D)** **DTSAM**: computational time interval to create output file [s] **WRITE_XYZ**: create a physical dimension file **QUANTITIES**: variables to include in the Plot3D output file
28	SmokeView Post-Processing Parameter (**&ISOF**) **QUANTY**: track &SPEC ID concentration **VALUE(n)**: concentration value of interest

7 VAPOR CLOUD FIRE

The second fire scenario of interest is one that occurs if the LNG is allowed to evaporate and disperse downwind before ignition. To calculate the thermal radiation resulting from this scenario, results from the dispersion modeling were used along with the burning vapor cloud methods described in Chapter 11 of the SFPE Handbook of Fire Protection Engineering [9]. As in the pool fire scenario, the thermal flux at any location is calculated using $\dot{q}'' = EF\tau$ where E is the emissive power of the flame, F is the view factor, and τ is the atmospheric transmissivity which is taken to be 0.8 here. The view factor was based on the data from Mudan [10] and the emissive power is taken to be 200 kW/m^2.

The vapor cloud fire differs from the pool fire primarily in the growth of the flame and how large the flame will be. For the pool fire, the flame width is essentially the diameter of the pool which also sets the flame height. For the vapor cloud, the size (or width) of the flame will growth with time up to a limit; the appropriate equations for calculating this growth are presented in the SFPE Handbook of Fire Protection Engineering [9].

The size of the flame will depend on the characteristics of the vapor cloud. The first case considered was the dispersed cloud in a 2 m/s wind field resulting from an intentional event. This was selected because it produced the longest downwind distances. The cloud shape and size were captured at various times to show the variation in hazard distance with time. The exact times were approximately 60, 72, and 90 minutes after the release. The 60-minute cloud represents the largest cloud area and will generate the largest hazard. The clouds produced at 72 and 90 minutes show how the hazard zone changes with time. They also provide information relevant to times earlier than the 60-minute mark since the cloud will be forming and will go through a similar shape change. The only difference will be the location of the cloud relative to the release point.

Key in setting the hazard zone is the size of the flame. Figure 9 shows the growth of the flame for the 60-minute cloud as calculated using the methods of the SFPE Handbook of Fire Protection Engineering [9]. It approaches a maximum width of approximately 950 m. For all analyses presented, this maximum width was used. This is the only option unless a time dependent analysis is performed. The flame height is a function of the width. Test data has shown the height to be approximately 40 percent of the width [9].

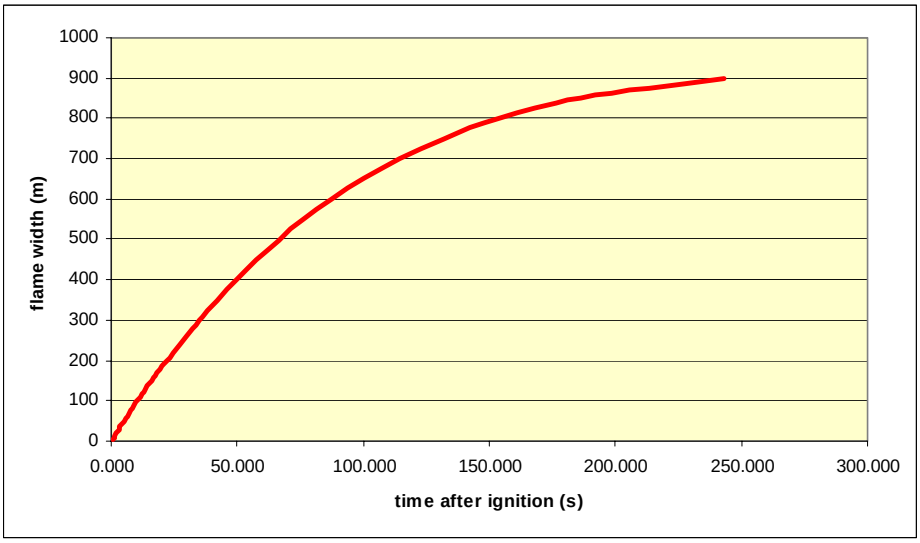

Figure 9. Flame width growth for the cloud at 60 minutes.

Two additional parameters are needed to make the calculation of flame width. The first is the propagation speed of the flame, based on available data (see Figure 3-11.42 of the SFPE Handbook of Fire Protection Engineering [9]). It would be approximately 5 m/s for the wind speeds of interest in this study. The other parameter is the upward velocity at the flame base, which was taken to be 0.16 m/s based on data for LNG.

Once the flame width and height is determined, the remaining variable is the location of the flame within the vapor cloud. This will depend on the ignition location. Since no specific ignition sources have been identified for this study, it was assumed that the flame location would produce the worst thermal loads at any point of interest. This required that the flame be positioned at the cloud boundary and moved around the perimeter as the flux receptor was moved. This is shown conceptually in Figure 10 where only two targets out of an infinite set of possibilities are shown.

In all cases, the flame is assumed to be situated at the edge of the cloud. This will produce the highest thermal loads in the field away from the cloud. The assumed flame location along with using the maximum flame width provides a conservative estimate of the thermal fluxes. As discussed in the SFPE Handbook of Fire Protection Engineering, the view factor needed is calculated using equations for non-titled rectangular flames [9].

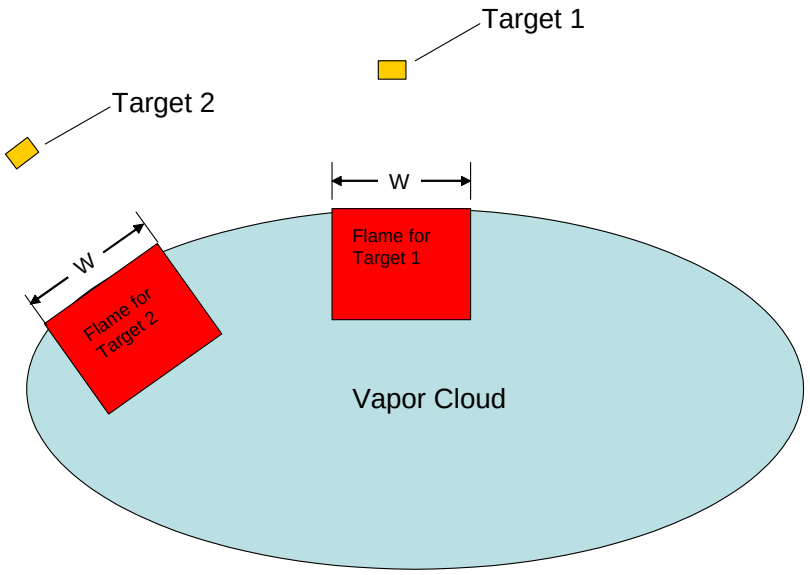

Figure 10. Conceptual notation of where the flame position was assumed for targets.

As mentioned previously, the thermal radiation loads will be directly tied to the cloud and flame size. Figure 11, 12, and 13 show the details of the clouds analyzed. The images show only half of the cloud since it is symmetric about the centerline. All dimensions are in meters. The figures demonstrate that the height of the cloud varies substantially across the cloud footprint with the maximum height is found along the centerline of the cloud. For simplicity this cloud height was assumed to be constant across the footprint of the cloud and the value used for the radiation calculation was taken to be the centerline value. For the vapor cloud at 60 minutes after release, the centerline cloud height was approximately 30 m.

Table 7. The distance from the edge of the cloud to radiative intensities of interest for the Intentional event involving two holes 7m^2 in size.

Heat Flux (kW/m^2)	Time After Release (min)		
	60	72	90
	Distance (m)*	Distance (m)*	Distance (m)*
37.5	400	270	150
12.5	870	550	310
5	1,440	930	510

* Distance is measured from the edge of the cloud.

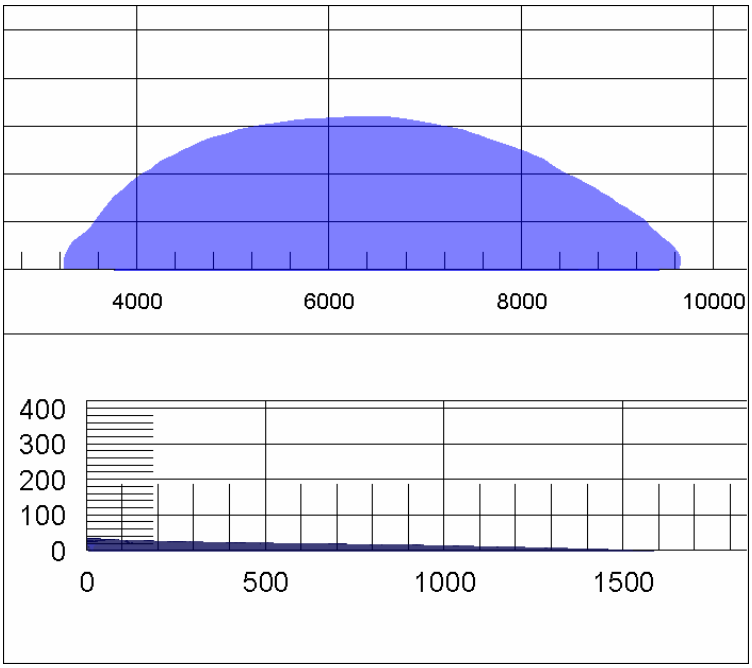

Figure 11. Cloud configuration at 60 minutes after release. Top: plan view. Bottom: side view.

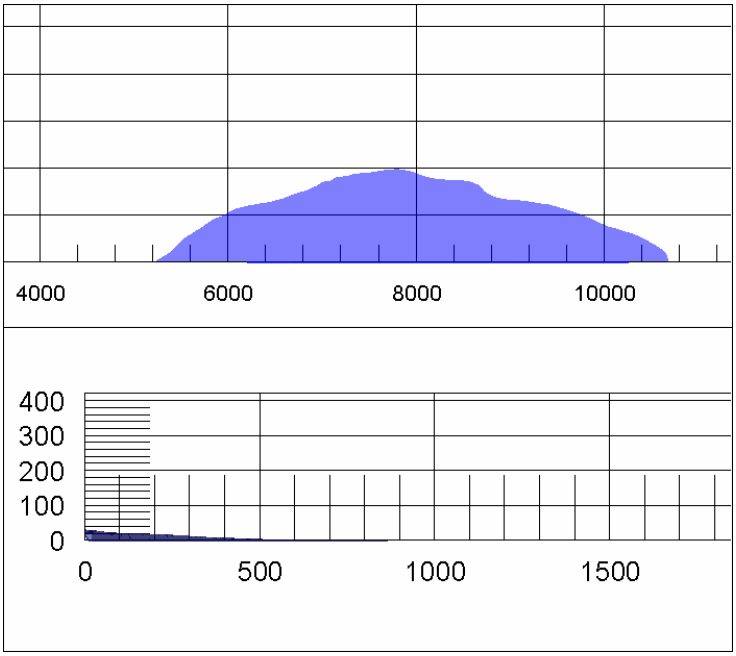

Figure 12. Cloud configuration at 72 minutes after release. Top: plan view. Bottom: side view.

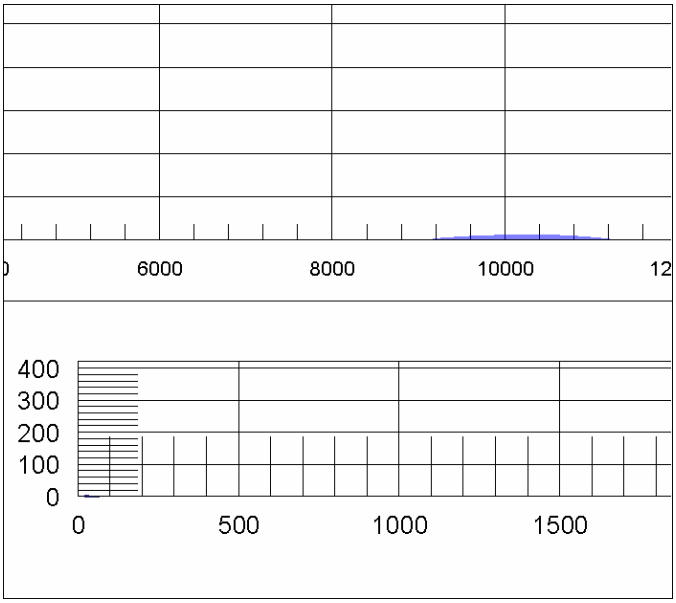

Figure 13. Cloud configuration at 90 minutes after release. Top: plan view. Bottom: side view.

At any location around the perimeter of the cloud, the thermal load will depend on the normal distance from the location to the cloud edge. The distances to key intensity levels are shown in Table 7. Figure 14 shows how the thermal load changes with this distance for the three clouds. The resulting radiative flux fields and clouds are shown in Figure 15, 16, and 17. This represents the thermal loads only at the instant in time corresponding to when the pool geometry was taken. However, the data presented includes the largest potential hazard and a good sample of the hazards at other times.

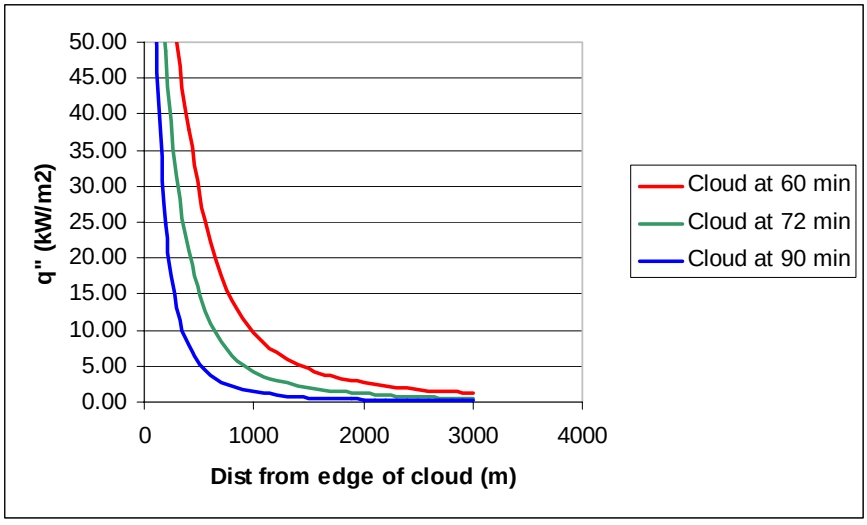

Figure 14. Thermal flux as a function of distance from the edge of the cloud for the three clouds considered.

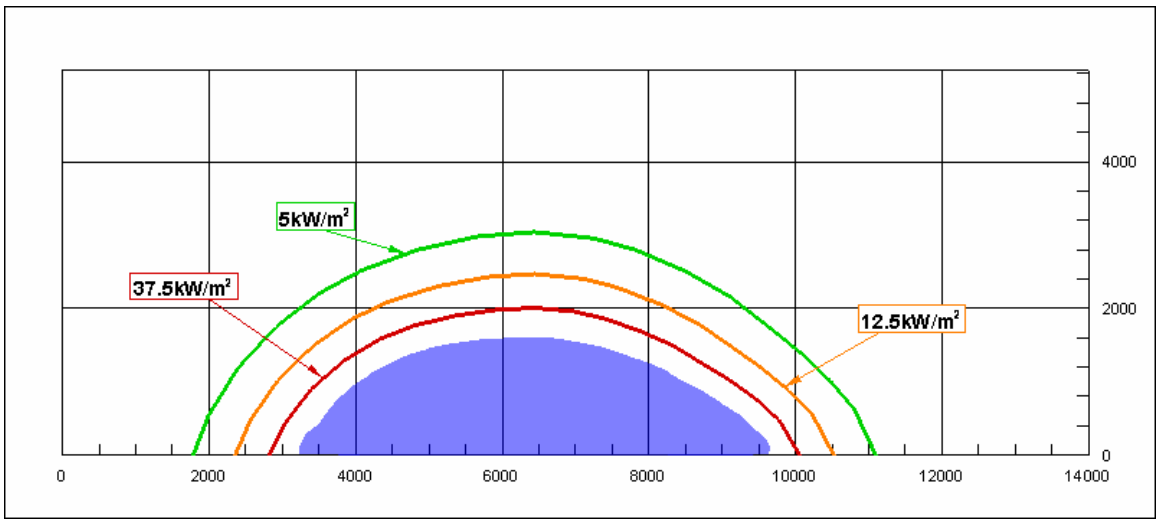

Figure 15. Thermal radiation data for the vapor cloud fire at 60 minutes.

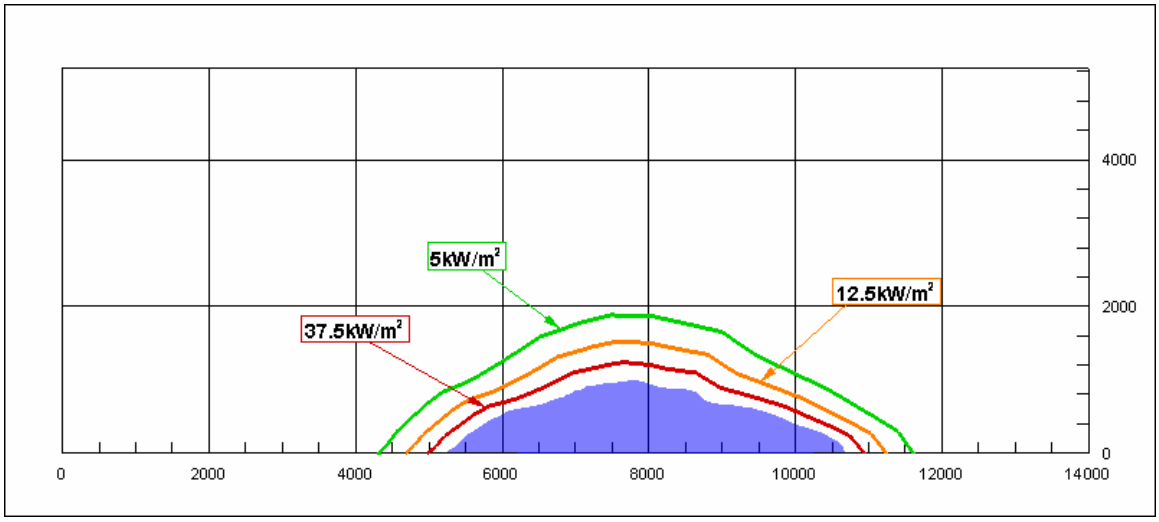

Figure 16. Thermal radiation data for the vapor cloud fire at 72 minutes.

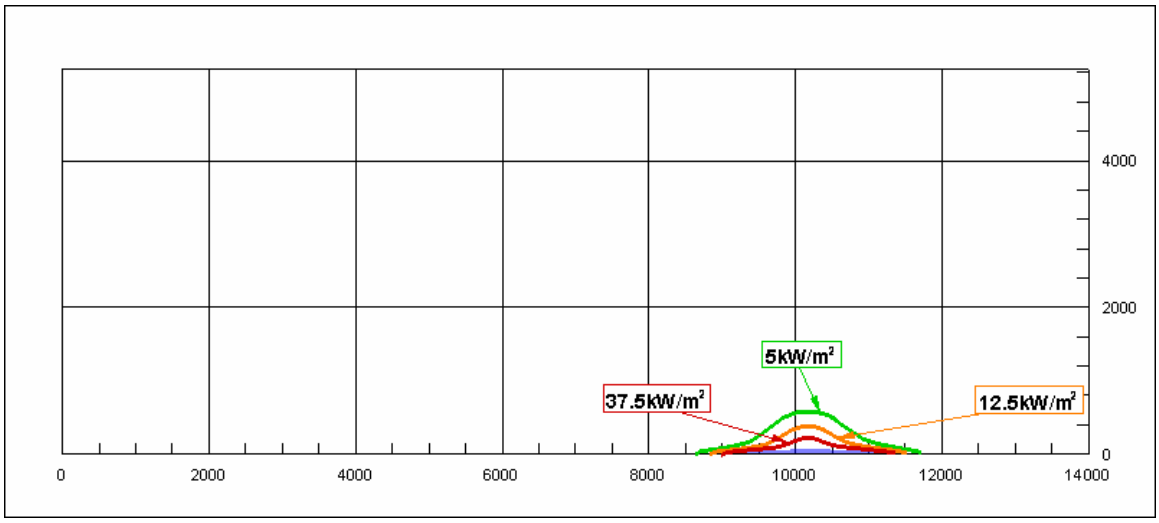

Figure 17. Thermal radiation data for the vapor cloud fire at 90 minutes.

The dispersion from the marine collision scenario was also considered. The largest cloud, shown in Figure 18, formed at approximately 50 minutes after the release. The height of the cloud at the centerline was approximately 21 m and this height was used for the radiation calculations. The radiation flux as a function of distance for this scenario is shown in Figure 19 and Table 8.

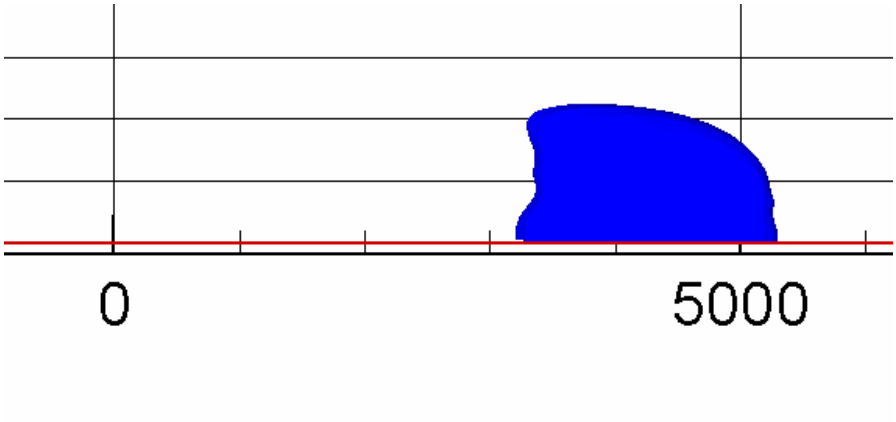

Figure 18. Footprint of the vapor cloud formed from the marine collision scenario. This represents the largest cloud volume.

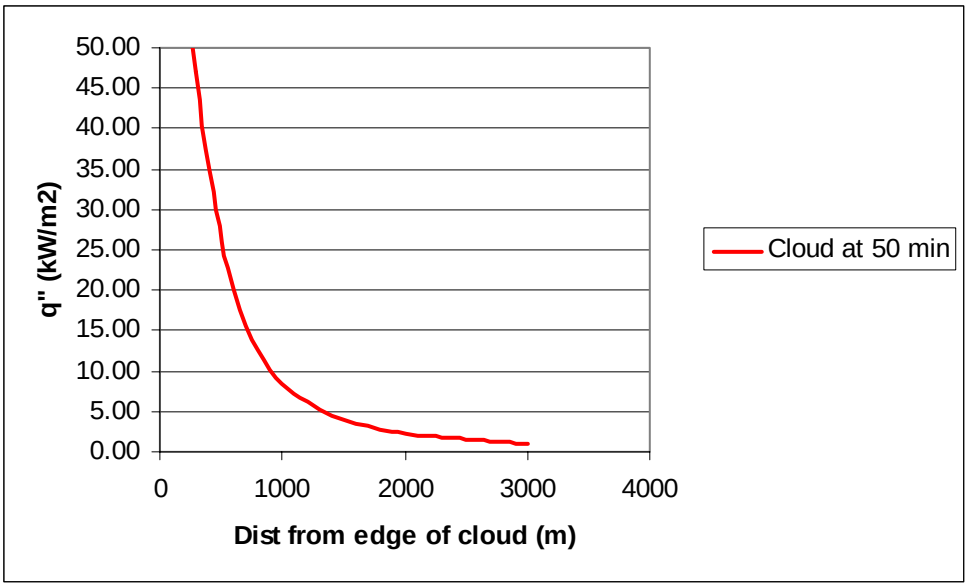

Figure 19. Thermal flux as a function of distance from the edge of the cloud for the largest vapor cloud formed as a result of the marine collision case.

Table 8. The distance from the edge of the cloud to radiative intensities of interest for the marine collision case.

Heat Flux (kW/m^2)	Distance (m)*
37.5	375
12.5	800
5	1,330

* Distance is measured from the edge of the cloud.

8 VAPOR CLOUD EXPLOSION

Another potential hazard of interest is a vapor cloud explosion. This could occur if the dispersed vapor cloud were ignited. To produce an explosion of any significance, the cloud has to interact with some level of congestion or confinement. Without this occurrence, a hard ignition such as an explosive charge would have to be employed to get any blast pressure of significance.

Various explosion scenarios were selected as a result of a workshop held in April 2004 regarding the Cabrillo Port LNG facility and the related license review. The purpose of this work was to calculate pressure load histories for various vapor cloud explosion scenarios. A CFD model known as Computational Explosion and Blast Assessment Model (CEBAM) was used to perform the modeling. Documentation and validation related to this model has been published by Clutter [11, 12, 13]. This model was selected over simplified methods to ensure that key phenomena such as blast focusing and channeling were included.

8.1 Scenario No. 1: Vapor Cloud Explosion in Hull Void Space without Venting

Scenario 1 analyzes the consequences of an explosion occurring in the void space between the FSRU hull and the spherical LNG cargo tank and bounded by the sphere skirt. The scenario assumes that a leak occurs in the void space that results in a stoichiometric flammable cloud that fills the entire volume between the cargo tank and the inside of the hull. Assuming a stoichiometric mix is conservative as regions that are rich or lean will reduce overall blast pressures. The specific cause of the leak is not defined for the purpose of consequence modeling. No venting of pressure is included in the simulation. This will result in overestimation of blast pressures as structural failures may lead to venting. Design details at the time of the study are insufficient to postulate venting behavior.

A worst-case assumption was made that a completely flammable cloud of methane and air fills the void space between the inner hull and the LNG sphere. This vapor cloud was then assumed to be ignited directly below the sphere, and cause a fast burn (deflagration) of the methane and air mix. The assumptions made in the CFD modeling were as follows:

- The entire confined volume between the inner hull and sphere was filled with a homogenous stoichiometric methane-air mix. This is a conservative assumption, as an actual mix would include regions of rich and lean material that will burn slower and contribute less energy than that of the optimum stoichiometric mix.
- Ignition occurred at the base of the LNG sphere.
- The flame speed for the combustion is set at Mach 0.29 (global reference frame) based on correlations presented in Baker [14].
- The hull, tank skirt, and sphere are non-responding over the explosion event time and, hence, do not move or change geometry.

The simulation was performed on one-quarter of the sphere and hull structure, taking advantage of existing symmetry conditions. Figure 20 shows the layout of the simulation and Figure 21 shows the probe locations inside the void space, where pressure time histories were recorded.

The probe data information is provided in Figure 22 and 23. Included are pressure-time histories and impulse-time histories. The highest pressure recorded at any probe location in the void space was directly under the sphere. The recorded pressure was approximately 115.5 pounds per square inch gauge (psig) (796.3 kilopascals [kPa]); however, all probes in the void space eventually reached this pressure as a result of the void space being sealed from the outside environment. The time to delay was 0.55 seconds for the peak pressure to be reached. Due to the length of rise time in pressure and the fact that the load is approximately uniform across the surface of the sphere, it is not likely that local damage such as holes in the spheres would be produced.

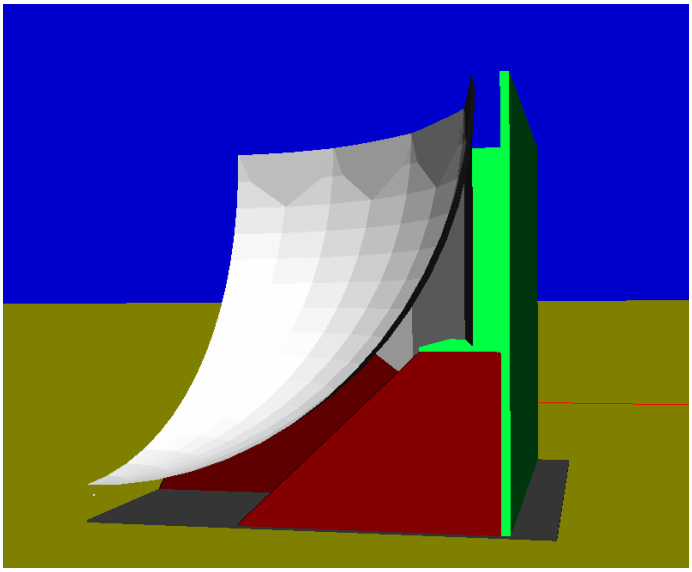

Figure 20. Geometry for the hull void space explosion scenario.

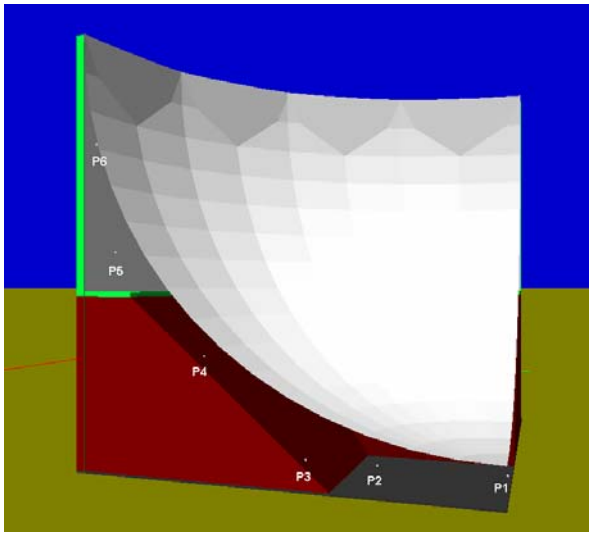

Figure 21. Probe locations in the void space.

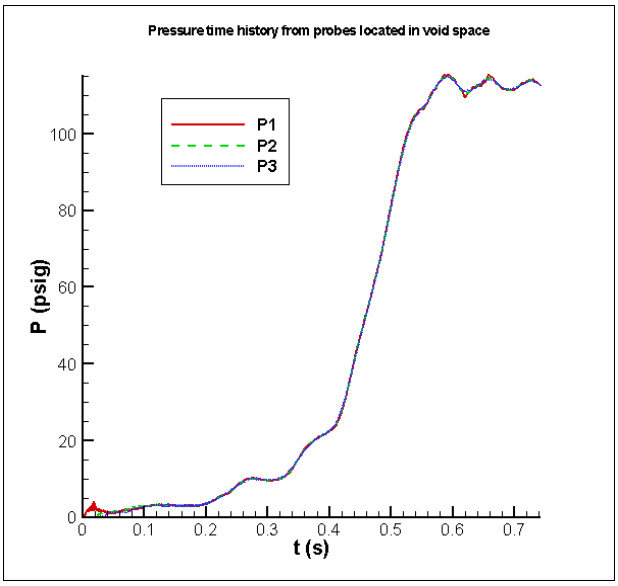

Figure 22. Pressure-time histories.

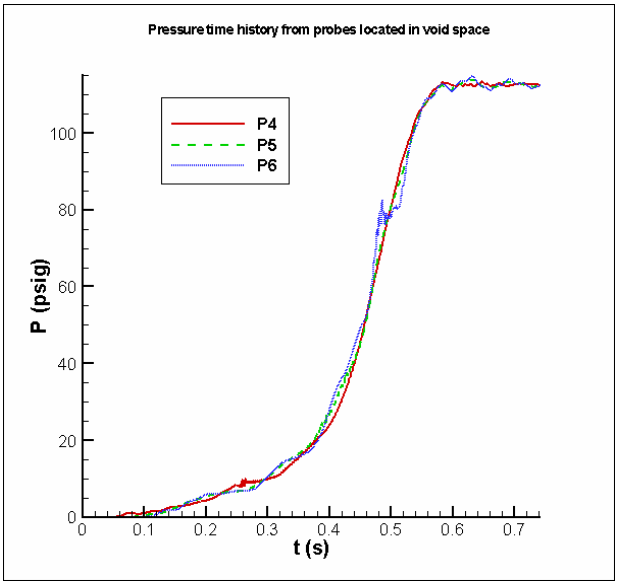

Figure 23. Impulse-time histories.

8.2 Scenario No. 2: Vapor Cloud Explosion in the Storage Spheres

Scenario No. 2 involves an explosion inside one of the LNG cargo tanks during maintenance, when the cargo tank is not being used to store LNG. The scenario assumes that methane is introduced into the cargo tank due to an accidental event and creates a flammable mixture that ignites. The following conditions are assumed for the analysis:

- The cargo tank is empty except for a stoichiometric mixture of methane and air and internal mechanical components.
- The cargo tank is non-responding and does not fail under the internal pressure.

- The cargo tank has no vents to the outside that would relieve gas pressure increase within the sphere.

The explosion of the LNG storage sphere was modeling using CEBAM. An eighth of the sphere was constructed within the computational domain. This was possible since three planes of symmetry could be utilized. An exterior view of the model is shown in Figure 24.

The sphere was filled with a stoichiometric mixture of methane and air at ambient pressure and assumed to be non-stratified. The fuel-air mixture within the sphere was ignited at the center of the sphere.

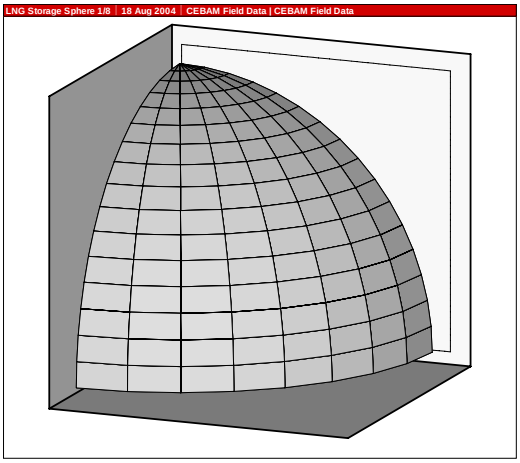

Figure 24. One-eighth section of LNG storage sphere.

The bulk of the sphere interior is open space and hence a low congestion condition would exist. National Fire Protection Association guidance [15] was used to define the flame speed for the CFD analysis. Figure B-1 of that document provides the effect of volume on the gas burn constant, K_G, for methane-air explosions in spherical vessels. K_G is a measure of how rapidly the pressure rises in the confined volume and is calculated using

$$K_G = (dP/dt)_{max} * V^{1/3}$$

Where: P = pressure
t = time
V = Volume
$(dP/dt)_{max}$ = maximum recorded pressure rise rate

The CFD modeling approach was used to construct the closed sphere in CEBAM and then fill the vessel with a methane-air mixture. CEBAM requires a flame speed as input to characterize the burning process rather than a K_G value. The simulation was run for a given burn rate and a pressure-time history was produced within the sphere. The K_G value was calculated using the equation above and compared with the published NFPA value. The flame speed was modified during several CFD iterations until good agreement between the K_G value and the measured

pressure-rise rate was obtained. The flame speed Mach 0.021 was found to match the expected K_G value.

The resulting pressure-time history in the closed sphere was obtained and is shown in Figure 25. It includes a relatively smooth rise in pressure up to a peak value of approximately 115 psi at around 6 seconds, with the peak pressure-rise-rate occurring between 4 and 5 seconds after ignition. There are some low level fluctuations that occur between 2 to 4 seconds and are caused by the flame front moving inside the sphere. Blast load profiles were developed and the important results are as follows:

- Maximum overpressure in void space: P_{max} = 115 psi (792.9 kPa)
- Rise time to peak overpressure: t_{peak} = 6 seconds

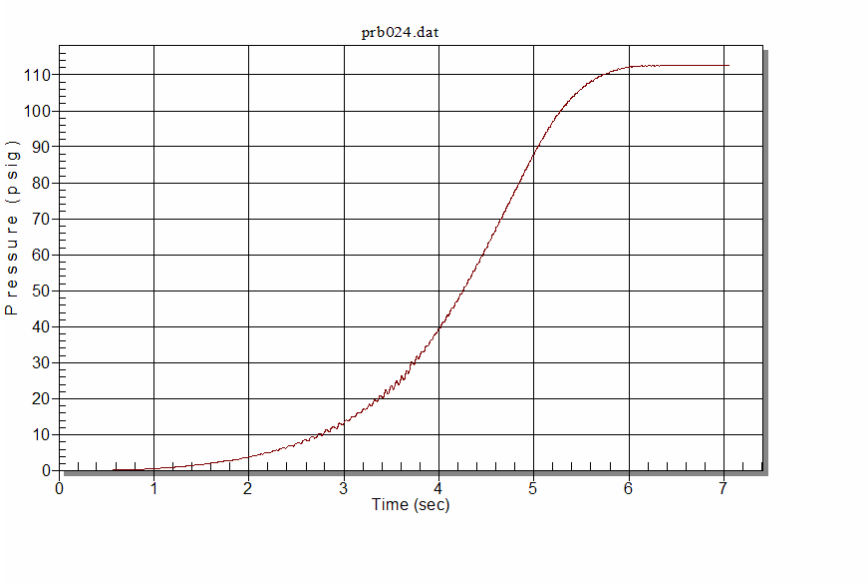

Figure 25. Pressure-time history of static pressure build-up within sphere.

8.3 Scenario No. 3: Vapor Cloud Explosion between the FSRU and an LNG Carrier

Scenario No. 3 analyzes the consequences of an explosion occurring between the FSRU and an LNG carrier during off-loading activities. The scenario assumes that the spill results in a stoichiometric flammable cloud that fills the entire space between the two floating platforms. This assumption of a spill that fills the full confined volume at optimum flammable conditions would have a greater result than other spill scenarios that result from leaks.

Because the LNG carrier and the FSRU are near one another during the loading process, an LNG leak release would cause heavier than air material to drop to the ocean surface between the two vessels. Heat transfer of the LNG from the water and confining vessels can cause rapid evaporation and heating of the resulting methane that will eventually rise and mix with air. A worst case assumption was made that a completely flammable cloud of methane and air fills the space between the two vessels. This vapor cloud was then assumed to be ignited and cause a fast burn (deflagration) of the built-up natural gas and air mix.

The confined volume between the LNG carrier and FSRU is approximately 240,000 ft^3 (6,800 m^3). A stoichiometric condition for a methane-air mix has 9.5 percent of the volume as methane and the rest as air. This is equivalent to approximately 23,000 ft^3 (650 m^3) of gaseous methane (based on Standard Conditions). The volume of LNG that when warmed to standard temperature and pressure (STP) conditions can produce that amount of gaseous methane is 36 ft^3 (1.0 m^3). This quantity or more of LNG product can be present in loading arms during operations.

The assumptions made in the CFD modeling were as follows:

- The entire confined volume between the LNG carrier and the FSRU was filled with a homogenous stoichiometric methane-air mix. This is a conservative assumption, as an actual mix would include regions of rich and lean material that will burn slower and contribute less energy than that of the optimum stoichiometric mix.
- Ignition occurred at the physical center of the cloud. This is considered conservative as this position results in the flame consuming the entire flammable cloud in the shortest period of time.
- The flame speed for the combustion is set at Mach 0.29 (global reference frame) based on correlations presented in Baker [14]. (A conservative assumption that was used in this selection is discussed further below.)
- The LNG carrier and FSRU are non-responding over the explosion event time and, hence, do not change move or change geometry.

An important CFD input parameter to select is the flame speed. This was selected based on Baker [14], which developed empirical correlations of flame speed based upon fuel reactivity, the type of confinement, and congestion conditions. The following conditions apply to this scenario:

- *Fuel reactivity:* Flammable vapors are classified into categories of low, medium, and high reactivity. Methane-air is considered low reactivity fuel based on its low laminar burning velocity and large detonation cell size. This is proven out by its relatively low energetic performance compared to other flammables under the same conditions. Low reactivity was selected for assigning flame speed.
- *Confinement:* Confinement type is classified into three groups. 3D-confinement is a situation where the reaction products, surrounding air, and blast pressures are free to expand in all directions. 2D-confinement is a condition where reaction products, surrounding air, and blast pressure are allowed to expand in only two directions, for example between two non-responding planes. 1D-confinement is a condition where reaction products, surrounding air, and blast pressures can expand in only one direction, for example within a pipe. The greater the confinement (toward 1D-confinement) the more violent the explosion. The region between the FSRU and the LNG carrier allows horizontal expansion in the stem-to-stern direction. Vertical expansion upward is allowed but not downward to the water surface. Also, transfer arms and mechanical equipment minimally restrict the upper direction. The hulls of the LNG carrier and FSRU block horizontal expansion. The conditions fall between that of 2D and 1D. The more conservative assumption of 1D-confinement was selected for assigning flame speed.

- *Congestion:* Congestion within the volume of the flammable cloud is classified as low, medium, and high. Congestion includes items such as piping, vessels, or other objects that occupy a percentage of the space and generates turbulence in the fuel-air mix as it is pushed ahead of the flame front. There is little or no such congestion between the FSRU and the Carrier. Low congestion was selected for assigning flame speed.

Based on the above conditions (low reactivity, 1D-confinement, and low congestion), a flame speed of Mach 0.29 (relative to the ground reference frame) was selected.

The simulation layout was an LNG carrier next to an FSRU. There is a 20-foot gap between the LNG carrier and the FSRU where the natural gas cloud builds up. Figure 26 shows the layout of the simulation. There is a natural gas vapor cloud between the LNG carrier and the FSRU. The black plane represents the water surface.

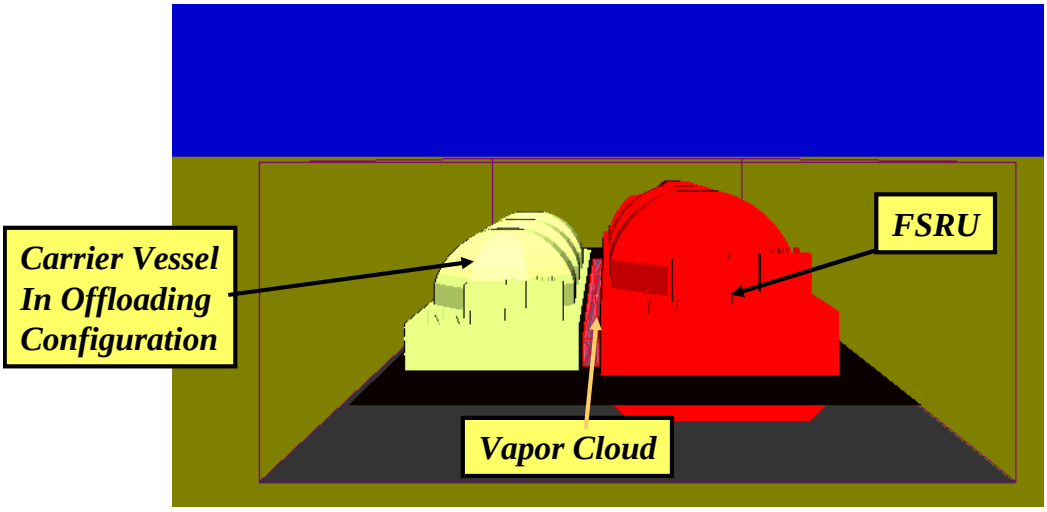

Figure 26. Scenario 3 simulation geometry.

An igniter was placed near the center of the cloud and a flame speed of Mach 0.29 was used to drive the energy release rate, selected as indicated above. Figure 27 shows the probe locations on both the FSRU and the LNG carrier. The probe locations were chosen to show the pressure and impulse history on the side of the storage tanks closest to the natural gas burning. Probes were also placed on the simulated water surface in the gas cloud longitudinal direction.

The probe data information is available for the following locations:

- Data probes located on the LNG carrier. Included are pressure histories on the surface of each of the three spheres that are facing the explosion.
- Data probes located on the FSRU. Included are pressure histories on the surface of each of the three spheres that are facing the explosion.
- Data probes located on the water surface.

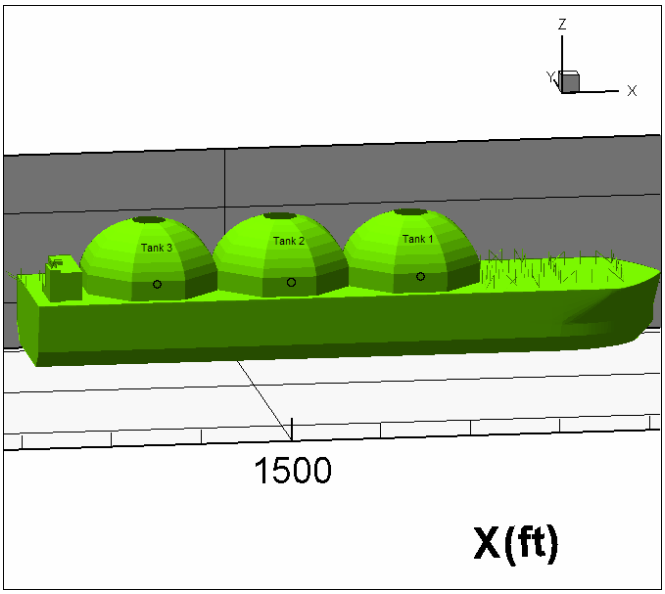

Figure 27. Probe locations shown as black circles.

Figure 28 is an example of these plots, showing the first 500 ms of pressure history at the probe locations on the three Moss tanks of the FSRU. This figure shows that the maximum overpressure occurs at Tank 2 (middle tank and closest to the center of the explosion) is approximately 3.5 psi (24 kPa). The corresponding impulse is calculated as the integral of the positive pressure phase, the crossed-hatched area in Figure 28, and has a maximum of approximately 145 psi per millisecond (-msec) (1.1 kPa per second [-sec]). The remaining plots are in Figure 29 through Figure 36.

The highest pressure recorded at any probe location in the domain was on the water surface near the vapor cloud center. This is a location that is in contact with the vapor cloud and where flow stagnates. The recorded pressure was approximately 13.5 psig (93 kPa). The recorded impulse at this location was approximately 480 psi-ms (3.3 kPa).

Blast pressure and impulse loadings were predicted in the following locations: (1) in the region between the LNG carrier and FSRU, (2) on the Moss tanks of the FSRU, and (3) on the LNG carrier's tanks. Approximate blast pressure and impulse results are as follows:

Blast between FSRU and LNG carrier: P_{max} = 13.5 psi (93 kPa), i_{max} = 480 psi-msec (3.3 kPa-sec)

Blast on LNG carrier tank: P_{max} = 3.5 psi (24 kPa), i_{max} = 160 psi-msec (1.1 kPa-sec)

Blast on FSRU sphere: P_{max} = 3.5 psi (24 kPa), i_{max} = 145 psi-msec (1.0 kPa-sec)

Where P_{max} is the peak blast overpressure and i_{max} is the positive phase specific impulse calculated as the integral of the positive phase blast pressure history.

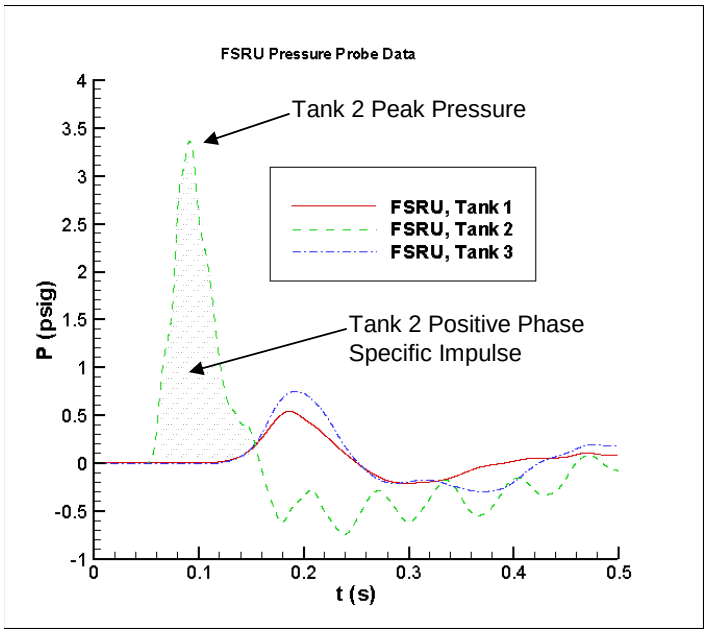

Figure 28. Load on FSRU spheres.

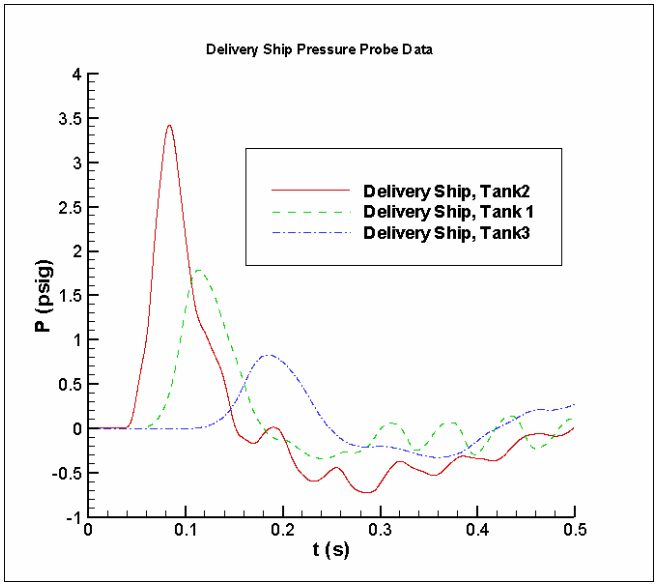

Figure 29. Delivery sphere pressure records.

Figure 30. Delivery sphere impulse data.

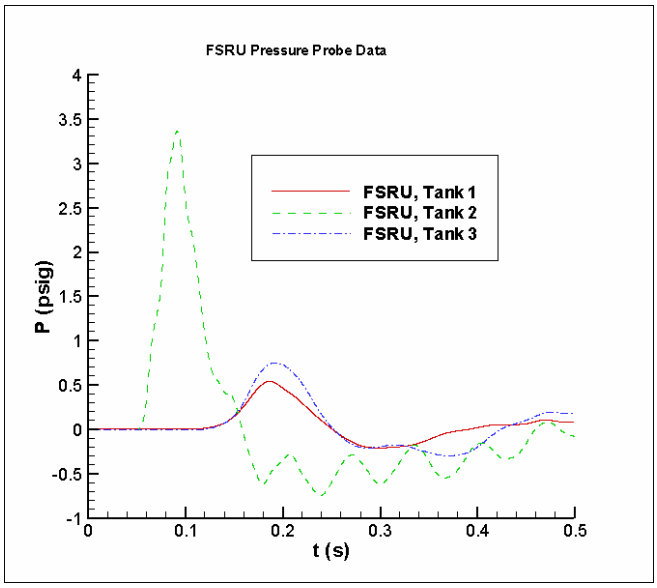

Figure 31. FSRU pressure probes.

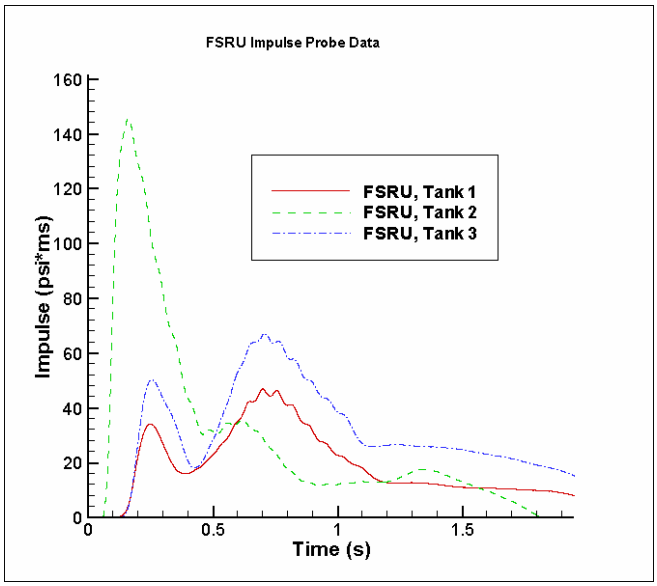

Figure 32. FSRU impulse data.

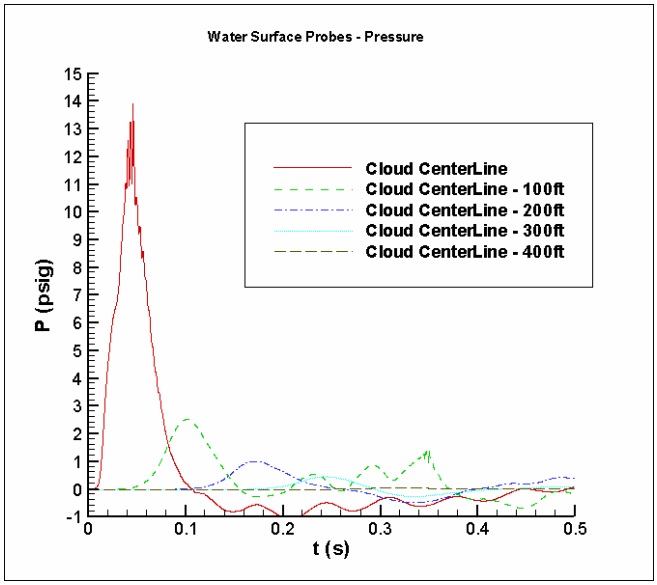

Figure 33. Water surface centerline pressure probes.

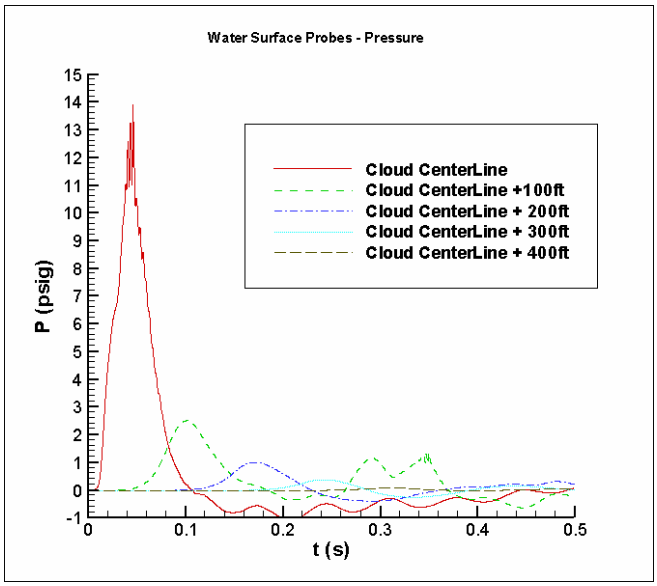

Figure 34. Water surface pressure probe data.

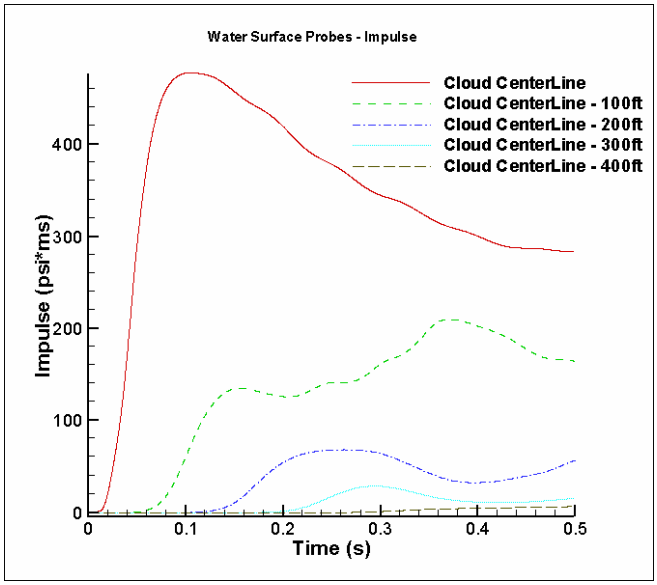

Figure 35. Water surface impulse data.

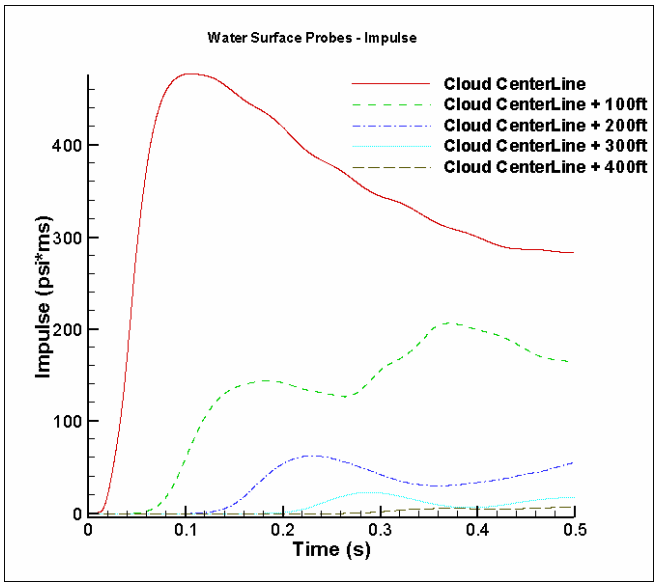

Figure 36. Water surface impulse data.

9 SUMMARY

The hazards produced from LNG spills at the proposed Cabrillo Port FSRU were analyzed and possible fires and explosions were considered. Four spill scenarios, including possible marine collision and intentional event scenarios, were modeled. The particular events and resulting hole sizes were defined as part of the Independent Risk Assessment to which this consequence analysis is an appendix.

The spilling and spreading processes were simulated using CFD technology, which allowed for the analysis of multiple spill events and captured the influence of all factors in the formation of the LNG pools. The volume of LNG spilled from the tanks ranged from 50,000 m^3 to 200,000 m^3. These spills produced pool sizes ranging in diameter from 610 m to 800 m.

If the pool resulting from the spill were ignited early in the event, a pool fire would result. For the predicted pool sizes, analytical pool fire models were used to determine the radiation hazards produced from these potential events. There is a direct correlation between radiation hazard distance and pool diameter. Distances to threshold radiation levels were determined. For the scenarios considered, the largest pool diameter was estimated to be 800 m which produced a distance to a radiative flux intensity of 5 kW/m^2 out to 3,230 meters.

Absent an ignition source, the LNG in the formed pool will begin to evaporate and disperse. CFD technology was used to simulate the dispersion of the evaporated gas. This technology allowed for the inclusion of key physical processes such as buoyancy effects. Prior to simulation of the specific Cabrillo cases, results from the CFD modeling tool used were compared to available experimental data with good results. The predicted downwind hazard distance for the benchmark case was within 14 percent of the test data.

The downwind dispersion distances produced by the different release scenarios were calculated. The pool size and inventory, as well as the environmental factors such as wind speed, affected the distances and were incorporated into the simulation. For these scenarios, the pool diameters ranged from 650 m to 730 m. The assumed wind conditions played an important role in the maximum distance to LFL. The predicted maximum distance to LFL ranged from 5,290 m to 11,175 m.

A vapor cloud fire can result from the formation of a vapor cloud. This event was simulated using analytical methods. The radiation hazard from a vapor cloud fire depends on factors such as the cloud size. Because the cloud changes with time, distinct instances after the release of the LNG were considered. For the instance when the vapor cloud was at its largest size, the distance to the lowest radiation level of interest was approximately 1,440 m, which represents the hazard distance from the edge of the cloud.

The final hazard involving released gas considered was explosions. Because explosions usually only occur where gases are confined, scenarios involving the FSRU were simulated. CFD technology was used to calculate the expected pressure loads from an explosion since that type of analysis includes blast amplification processes such as focusing and channeling. Of interest were the pressure loadings within the facility and away from the FSRU. The pressures are found to decay quickly at distances away from the FSRU and no significant blast hazard is expected off-site. No structural analysis was conducted using the predicted explosion loads.

10 REFERENCES

1 Havens, J., Spicer, T., "LNG Vapor Dispersion Prediction with the DEGADIS Dense Gas Dispersion Model," Gas Research Institute, September 1990.

2 Hightower, M., Gritzo, L., Luketa-Hanlin, A., Covan, J., Tieszen, S., Wellman, G., Irwin, M., Kaneshige, M., Melof, B., Morrow, C., Ragland, D., Guidance on Risk Analysis and Safety Implications of a Large Liquefied Natural Gas (LNG) Spill Over Water, SAND2004-6258, Sandia National Laboratories, December 2004.

3 McGrattan, Kevin B., "Fire Dynamics Simulator, Version 4," NIST Special Publication 1018.

4 Chang, C., Meroney, R., Concentration and Flow Distributions in Urban Street Canyons: Wind Tunnel and Computational Data, *Journal of Wind Engineering and Industrial Aerodynamics*, 91 (2003) 1141-1154.

5 Clement, J.M., Experimental Verification of the Fire Dynamics Simulator (FDS) Hydrodynamic Model, PhD Thesis, University of Canterbury, Christchurch, New Zealand, October 2000.

6 Koopman, R.P., J. Baker, et al.," LLNL/NWC 1980 LNG Spill Tests. Burro Series Data Report" Lawrence Livermore Laboratory, December 1982, UCID-19075-Vol.1.

7 Luketa-Hanlin, A., Sandia National Laboratories, personal communication, October 2005.

8 Raj, P.K., "Models for Cryogenic Liquid Spill Behavior on Land and Water," *Journal of Hazardous Materials*, 5 (1981) 111-130.

9 Society of Fire Protection Engineers (SFPE) Handbook of Fire Protection Engineering, 3rd Edition.

10 Mudan, K.S., Geometric View Factors for Thermal Radiation Hazard Assessment, *Fire Safety Journal*, 12 (1987) 89-96.

11 Clutter, J.K., and Luckritz, R.T. "Comparison of a Reduced Explosion Model to Blast Curve and Experimental Data," *Journal of Hazardous Materials*, Vol. 79, October 2000, pp. 41-61.

12 Clutter, J.K., "A Reduced Combustion Model for Vapor Cloud Explosions Validated Against Full-Scale Data," *Journal of Loss Prevention in the Process Industries*, Vol. 14, Issue 3, February 2001, pp. 181-192.

13 Clutter, J.K., and Mathis, J., "Computational modeling of vapor cloud explosions in off-shore rigs using a flame-speed based combustion model," *Journal of Loss Prevention in the Process Industries*, Vol. 15, Issue 5, September 2002, pp. 391-401.

14 Baker, Q.A., Tang, M.J., Scheier, E.A., G.J. Silva, "Vapor cloud explosion analysis," *Process Safety Progress*, Vol 15 No. 2 1996 106–109.

15 National Fire Protection Association (NFPA) Guide for Venting of Deflagrations, 2002 edition, NFPA 68.